ARTICLE INFO
Received : August 22, 2023
Revised : October 18, 2024
Accepted : Octobre 21, 2024
CT&F - Ciencia, Tecnologia y Futuro Vol 14, Num 2 December 2024. pages 29-44
DOI: https://doi.org/10.29047/01225383.656

ctyf@ecopetrol.com.co

STRUCTURAL INSIGHTS OF ASPHALTENES THROUGH MILD OXIDATION REACTIONS AND MID INFRARED SPECTROSCOPY

USO DE LA OXIDACIÓN SUAVE ACOPLADA A ESPECTROSCOPIA DE INFRARROJO MEDIO PARA OBTENER PARÁMETROS ESTRUCTURALES DE ASFALTENOS

Fernando A. Rojas-Ruiz [1]; Diego R. Merchan-Arenas[1]; Santiago Villabona-Estupiñan[2]; Juan S. Ramírez-Pradilla[1]; Jorge A. Orrego-Ruiz[1].*

ABSTRACT
Mild oxidation reactions were induced over four different asphaltenes. Oxidation products were characterized via infrared spectroscopy to propose structural descriptors, taking advantage of the high sensitivity for detecting carbon oxygen vibrations in the infrared spectrum. Although no quantification over functional groups was performed, a good comparison between feedstock and products was achieved, after de-convoluting the FTIR spectra. It was confirmed that methyl groups are useful moieties on tracing the position of alkyl topologies over the n-heptane insoluble structures throughout oxidation reactions, as oxidation is more suitable on α-H of side alkyl chains. Considering this, it was inferred that the esters were the main functional groups formed under such oxidation conditions. The formation of lactones over aromatic nuclei was monitored through the slope of a parity plot with band intensity ranging between 1730cm^{-1} and 1230cm^{-1}. TGA-MS and ^{1}H-NMR analysis of raw n-heptane insolubles rendered valuable complementary information to confirm the structural attributes of the samples obtained by FTIR. The results from this research prove that handling oxidation selectivity over such complex hydrocarbon mixtures could have broader relevance for structural characterization purposes.

RESUMEN
Cuatro asfaltenos fueron sometidos a reacciones de oxidación suaves. Los productos de oxidación se caracterizaron mediante espectroscopía infrarroja para proponer descriptores estructurales, aprovechando la alta sensibilidad para detectar vibraciones de carbono y oxígeno en el espectro infrarrojo. Aunque el trabajo no se enfocó en cuantificar grupos funcionales, se logró una buena comparación entre la materia prima y los productos, después de de-convolucionar los espectros FTIR. Se confirmó que los grupos metilo son fragmentos útiles para rastrear la posición de las topologías alquílicas sobre las estructuras de asfaltenos durante las reacciones de oxidación, ya que la oxidación es más adecuada en α-H de las cadenas de alquilo laterales. Considerando lo anterior, se pudo inferir que los ésteres fueron los principales grupos funcionales formados bajo las condiciones de oxidación empleadas. La formación de lactonas sobre núcleos aromáticos se monitoreó a través de la pendiente de un diagrama de paridad entre las intensidades de las bandas alrededor de 1730 cm^{-1} y 1230 cm^{-1}. Los análisis TGA-MS y de RMN-H1 ofrecieron ofreció información valiosa que contribuyó a confirmar los atributos estructurales de las muestras obtenidos por FTIR. Los resultados obtenidos en esta investigación demuestran que el manejo de la selectividad de oxidación sobre mezclas de hidrocarburos tan complejas podría tener una relevancia más amplia que se extiende más allá del uso de procesos de oxidación para la mejora de asfaltenos, hacia propósitos de caracterización estructural.

KEYWORDS / PALABRAS CLAVE
asphaltenes characterization | asphaltenes oxidation | reactivity-structure relationship
Caracterización de asfaltenos | Reacciones de oxidación sobre asfaltenos | Relación espectro composición.

AFFILIATION
[1]ECOPETROL, Instituto Colombiano del Petróleo y energías de la transición ICPET, Piedecuesta, Santander Colombia
[2]Desarrollo en tecnologías de Hidrocarburos SAS, Piedecuesta, Santander, Colombia
*email: fernandoa.rojas@ecopetrol.com.co

1. INTRODUCTION

Asphaltenes are the most polar fraction of petroleum, obtained as dark solids by either treating crude oils with low-boiling paraffins (González et al., 2006) by dropping pressure in alive crudes (Klein et al., 2006), or by an ultra filtration process (Zhao & Shaw, 2007) They have been broadly defined as the fraction of crude oil insoluble in paraffins (usually n-heptane or n-pentane) although soluble in aromatic solvents like toluene and benzene and, specifically, according to the ASTM-6560-22 as the crude oil fraction insoluble in n-heptane and soluble in toluene (ASTM Standard D6560-22, 2022). This definition is given by their behavior rather than by any specific chemical classification. Therefore, understanding the composition and structure of asphaltenes is crucial for diagnosing, preventing and/or even predicting several of the more costly problems throughout the entire oil industry value chain, such as clogging of transport/production lines and equipment, catalyst deactivation, among others. In this sense, several techniques such as infrared spectroscopy (IR) (Asemani & Rabbani, 2020; Gargiulo et al., 2015, Gargiulo et al., 2016; Russo et al., 2014; Zojaji et al., 2021) matrix assisted laser desorption/ionization mass spectrometry (MALDI/TOF) (Zheng et al., 2018) ultra-small-angle X-ray scattering (Yang, et al, 2018) X-ray diffraction (XRD) (Díaz-Sánchez et al., 2017) nuclear magnetic resonance (NMR) (Ok & Mal, 2019) Fourier transform ion cyclotron resonance mass spectrometry (FT-ICR MS) (Pudenzi et al., 2018) atomic force microscopy (AFM) (Schuler et al., 2015) have been used in asphaltenes' characterization. These techniques have focused on establishing average molecular weights, determining functional groups and, thereafter, proposing molecular structures containing most of these features (Fakher et al., 2020; F. Zheng et al., 2020; Zuo et al., 2019) A significant number of papers have been published on the subject, in which almost all the available spectroscopic and spectrometric techniques have been employed (Fakher et al., 2020; Zendehboudi, 2019; Zheng et al., 2020; Zuo et al., 2019). Regarding the molecular weight, it seems like the longstanding controversy over whether it is thousands or hundreds of Dalton's was left behind with the overwhelming advances in mass spectrometry (Hortal et al., 2007) and atomic force microscopy techniques (Schuler et al., 2015). Concerning the molecular architecture of asphaltenes, Yen-Mullins suggests that fraction precipitated with n-C_7 have an exclusively condensed polyaromatic structure, called "island". The most probable molecular weight of an asphaltene molecule is ~750 g/mol, and the "island" molecular architecture corresponds to a system that fluctuates between 5 and 8 aromatic rings per molecule (Mullins, et al., 2012). On the other hand, some authors have proposed that asphaltenes can be made up of both island and archipelago-type structures. An archipelago-like structure suggests that asphaltenes contain more than one aromatic nucleus bonded by alkyl or cycloalkyl bridges (Chacón-Patiño et al., 2018; Chacón-Patiño, et al., 2017)

Regarding the main characteristic of the fraction precipitated with n-C_7, -their aggregation- this is a process where numerous compounds are involved. The great interaction between asphaltenes and the rest of the molecules of the oil are the cause for compounds with high affinities with asphaltenes (but soluble in n-heptane), to finally co-precipitate with them (Liao et al., 2005; Ganeeva, et al., 2021). The presence of these compounds (co-precipitated molecules) within the fraction precipitated with n-C_7 makes their characterization more difficult, as these compounds can lead to misunderstanding the results, adding or subtracting either molecular weight or functionalities, mimicking important structural features (Orrego-Ruiz et al., 2022). Thus, resolving the "asphaltenes puzzle" through studying structure, composition, and aggregation behavior, remains being an open window in several scientific fields.

An accurate way for analyzing complex organic matter is throughout chemical transformations and obtaining molecular information from their products (Derenne & Nguyen Tu, 2014), which has been demonstrated for lignin (Evstigneyev & Shevchenko, 2019) fulvic and humic acids (Klučáková et al., 2000) coal (Liotta et al., 1981) among others. In the case of asphaltenes, chemical transformation has gained momentum as strategy for their assessed to figure out the arrangement of the aromatic cores using the ruthenium-ion catalyzed oxidation (RICO) (Strausz et al., 1999). On the other hand, methylation reactions have been proved to explain the disaggregation effect due to the decrease in hydrogen bonds connecting its molecules (Bian et al., 2019). In another research, the reactivity of asphaltenes was studied through the Friedel-Craft reaction catalyzed by FeCl3 with the aim of obtaining liquid fuels. (Klerk, 2015). Additionally, in an attempt to improve its solubility in organic solvents, alkylation reactions were performed on asphaltenes seeking to break the C-S and C-O bonds. (Cagniant et al., 2001). For characterization purposes, oximation and imination reactions were developed on asphaltenes, aimed at the identification of carbonyl groups (Thorn & Cox, 2015). Other chemical transformations have been explored in fractions precipitated with n-C_7 studies highlighting chlorination (Siddiqui, 2009) bromination (Spiegel et al., 2018), and silylation (Desando & Ripmeester, 2000) among others. One of the most interesting and little explored chemical modifications is the oxidation reaction developed under mild reaction conditions. A well-designed procedure for oxidation using H_2O_2/CH_3COOH was proposed for releasing trapped compounds in asphaltenes with geo-chemical purposes. Such compounds are selectively oxidized within the aggregates, presumably without altering peripheral alkyl sidechains of asphaltenes (Liao et al., 2005) On the other hand, it was found that oxidized asphaltenes have a marked aggregation tendency by increasing viscosity (Oldham et al., 2020). Medina, et al. explored the thermal oxidation of an asphaltene, varying pressure, heating ratio, and the amount of material. The authors found that asphaltenes exhibited several combustion profiles at different temperatures, which suggests partial conversion of the residue as a function of the system pressure. (Medina, et al., 2019) Kök, et al. reported the use of TGA-MS for the analysis of volatile species generated from crude-oils during the thermal analysis (H2, H_2O, CO_2, etc,), finding strong differences between samples (Kök, et al., 2017). The combination of several analytical techniques has demonstrated to be the most robust option on asphaltenes' structure studies (Elbaz et al., 2015; Qiyong et al., 2020). However, recently in a different contribution, engaging analytical results obtained by FT-IR have shown complementarity with complex techniques such as NMR, TGA-MS and FT-ICR MS, affording a global but accurate vision of different Colombian asphaltenes' structure (Ramírez-Pradilla et al., 2024).

In 2016, our group proposed a successive Soxhlet extraction (n-heptane)–maceration procedure to obtain fractions enriched in trapped compounds that were originally within the macroporous structures of asphaltenes (Chacón-Patiño et al., 2016). In such work, the composition of trapped compounds (occluded) was

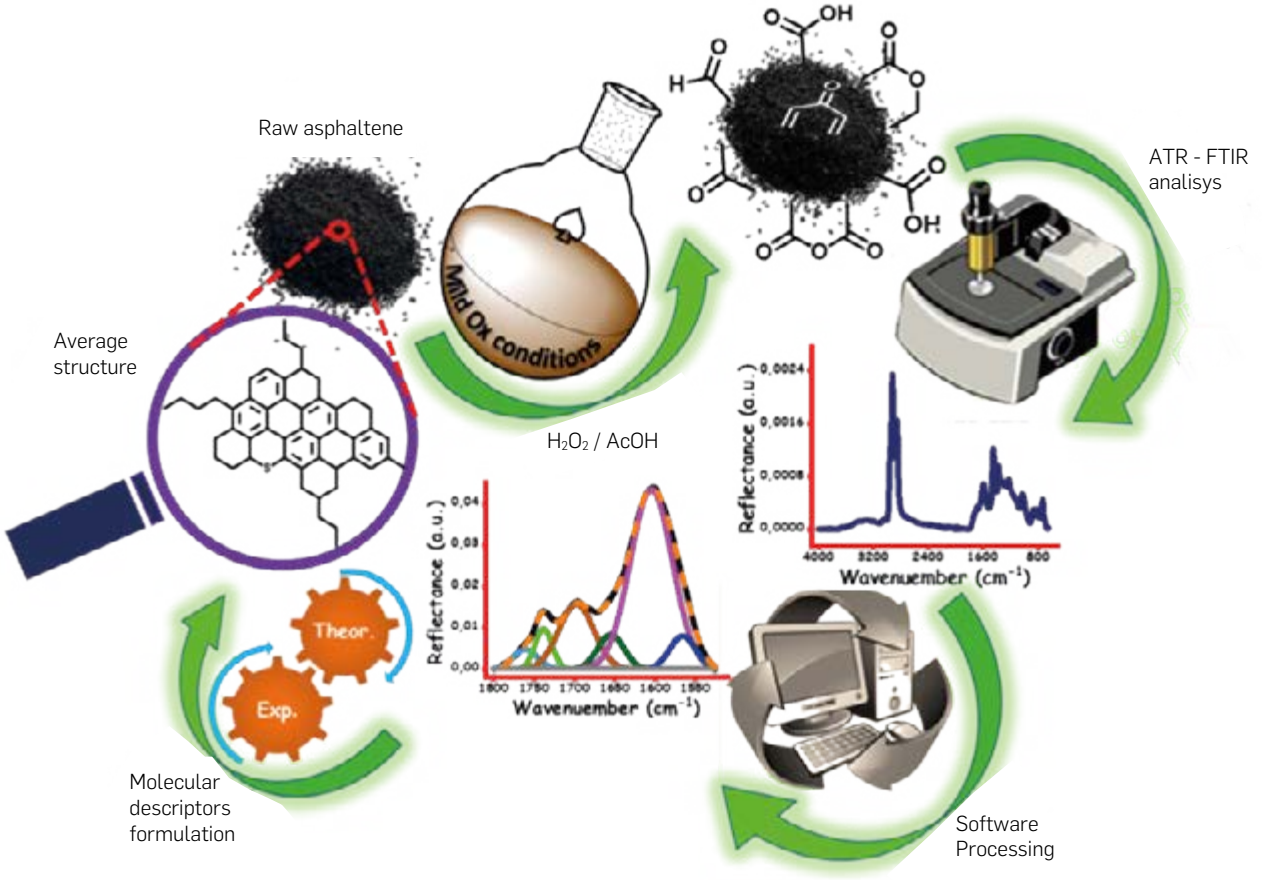

Figure 1. Analytical protocol developed for structural analysis of asphaltenes

examined, and it was evidenced that an important amount of n-C_7 soluble fraction (up to 15%) can be accounted as asphaltenes, altering the real composition of this fraction. Bearing this in mind, a similar extraction method is now proposed to obtain occluded-free asphaltenes, which can be further characterized via the analysis of their oxidation products. Thus, mild oxidation reactions were performed over four C_7 asphaltenes, obtained from different crude oils, knowing that the asphaltenes are prone to oxidize due to their highly aromatic structures, alkyl moieties, and content of heteroatoms (Chacón-Patiño et al., 2020; Kovalenko et al., 2020; Llanos et al., 2018; Rojas-Ruiz et al., 2017). Taking advantage of the high sensitivity for carbon–oxygen vibrations in the infrared spectrum (Sánchez & de Klerk, 2016a), oxidation products were characterized, and their original structure was assessed based on specific spectra-structural parameters. Although no quantification was performed, a good comparison was achieved between reaction feedstock and products after de-convoluting the FTIR spectra. Furthermore, TGA MS and 13C/^{1}H NMR analysis of raw asphaltenes rendered valuable information to confirm the structural attributes of the samples obtained by FTIR. The results obtained from this research prove that handling oxidation selectivity over such complex hydrocarbon mixtures could have broader relevance beyond the use of oxidation processes for asphaltenes upgrading (Sánchez & de Klerk, 2016a) for structural characterization purposes. Figure 1 summarizes the analytical protocol developed in this research.

2 EXPERIMENTAL DEVELOPMENT

MATERIALS AND METHODS

The crude oils from which the fraction precipitated with n-C_7 under study come correspond to some of the most representative fields in Colombia. Names were encoded for confidential reasons. Such oils were characterized according to the following procedures. API Gravity and Total Acid Number (mg KOH/g) were determined for the crude oils from which the asphaltenes were obtained, according to ASTM D287 and ASTM D664 methods, respectively. Toluene and heptane analytical grade (>99% Merck Chemicals) were used as solvents for sample preparation. Oxidation reactions were developed using reagent grade hydrogen peroxide (30% (w/w) in H_2O; Sigma Aldrich) and glacial acetic acid (AcOH; ReagentPlus® ≥99% Sigma Aldrich).

ASPHALTENE OBTENTION

Fraction precipitated with n-C_7 were obtained as follows. In short, 400 mL of n heptane were added dropwise to 10 g of crude oil, under sonication. The crude-heptane mixture was left under sonication for 2 h and then left overnight. The insoluble fraction was then collected

by filtration (Whatman 42) and placed in a Soxhlet apparatus with n-heptane for 48 h. The precipitate was removed, and its weight registered once it reached constant weight. The sample was gently crushed using a glass vial, avoiding potential damage in the sample for localized overheating, and placed in the Soxhlet for an additional 24 h (72 h wash). The same procedure was repeated up to 96 h to obtain n-C_7 insoluble washed and free of trapped compounds. That is, the drying, maceration, and weighing procedure was repeated once every 24 h until completing a total of 96 h of washing completed (Chacón-Patiño et al., 2016). The elemental analysis of the n-C_7 insoluble 96h was carried out following the ASTM method D5291–16 for carbon, hydrogen, and nitrogen, and the ASTM method D1552–16 for sulfur.

OXIDATION REACTION

Oxidation reactions were developed according to a modified protocol reported by Liao and co. (Liao et al., 2006). Briefly, 21 µL of H_2O_2 with 206 µL of glacial acetic acid (AcOH) in a 10 mL vial were mixed for around 10 min. Furthermore, 50 mg of n-C_7 insoluble were diluted in 3.0 mL of toluene and then added to the reaction vial. Temperature was tested during the process. The reaction under room temperature (20 °C) was labeled as O1, and the reaction under 60 °C as O_2. After 3 h, 5 mL of water were added to the reaction mass, and the whole mixture extracted with dichloromethane (DCM) (5 mL, 2 times). The organic phase was collected over Na_2SO_4, and then filtered through a cotton path. The resulting organic phase was concentrated by evaporation. The water phase (water + dissolved organic material + Na_2SO_4) was not considered for further analysis. Oxidized n-C_7 insolubles were obtained as black solids.

INFRARED SPECTROSCOPY MEASUREMENTS

Samples were characterized using a Bruker-alfa spectrometer in attenuated total reflection (ATR) mode using a diamond cell with a single reflection (45°). The spectra were acquired by accumulation of 32 scans, over a range of 4000- 650 cm^{-1} and a resolution of 4 cm^{-1}. The spectrometer was equipped with a deuterated triglycine sulfate (DTGS) detector. Background of the air was collected for every sample before its acquisition. Samples diluted in dichloromethane (DCM) were spread on the diamond cell, and once the signals of the solvent disappeared, the spectrum was collected. Then, baseline correction and area normalization were performed. All the spectra were exported in ASCI mode to be processed using multiple Peak Fit tools of OriginPro software version 9.3.

DECONVOLUTION TREATMENT

Each spectrum was sectioned into four regions (3000-2750, 1800-1540, 1070-960 and 900 700 cm^{-1}). For the adjustment of the curves, the Levenberg Marquardt iteration algorithm was used. Different peak shapes were evaluated in each region. Gaussian and Lorentzian yielded better adjustments than Giddings, Pearson and Voigt functions, which is consistent with previous works. The number and position of the peaks used in the fitting procedure were supported in data reported in the literature for crude oil, asphaltenes, coals (Ramirez-Pradilla et al., 2024)]. Kerogen and Bitumen and other carbon-based materials. The quality of the adjustments was evaluated visually and statistically by considering the values of the reduced chi-squared and the correlation coefficients (R2).

THERMOGRAVIMETRIC AND MASS SPECTROMETRY ANALYSIS

For thermogravimetric (TGA) analysis, a METTLER/TOLEDO TGA 3+ instrument (Columbus, OH, US) equipped with a thermobalance and alumina pan (150 µL), was used. Approximately 10 mg of each sample were subjected to a temperature ramp from 25 °C to 600 °C under air atmosphere (50 mL/min) and a rate of 10 °C/min; a plateau of 10 min at 600 °C was set for complete combustion/oxidation of the fraction precipitated with n-C_7. For the mass spectrometry analysis, a PFEIFFER THERMOSTAR GSD-350 (Asslar, GE) instrument, equipped with a quadrupole and a heated interphase, was used. For a typical running, the interphase was heated up to 200 °C to prevent sticking in capillary inlet, a vacuum of $1x10^{-9}$ Bar, 2 s/scan, and inlet temperature of 80 °C, were used.

^{1}H NMR ANALYSIS

^{1}H- spectra were obtained in a Bruker Avance III instrument at 400.16 and 100.62 MHz, respectively. The concentration of the samples was 4% by weight in deuterated chloroform $CDCl_3$ (99.8%D) for ^{1}H-NMR, and 20% by weight in $CDCl_3$ (99.8%D) using 0.05M $Cr_{(acac)}$ as paramagnetic relaxant. The acquisition for ^{1}H-NMR spectra was by accumulation of 16 scans using Bruker's zg30 pulse sequence (30° pulses), with a relaxation time of 10s. The spectra were acquired on a 5 mm probe at a temperature of 298.15 K. The assignments of the NMR bands, as well as the integration of the bands of interest, were carried out following the procedure described in the work of Poveda & Molina (2012).

3. RESULTS & ANALYSIS

SAMPLES CHARACTERIZATION

Table 1 summarizes the properties of the crudes from which the asphaltenes were extracted. The crude oils had a wide API range from 9.4 to 29.8, which reflects the asphaltene content, fluctuating from 0.61 to 8.7%. The acidity of the samples varied between TAN values of 0.1 and 5.7 mg KOH/g oil.

Table 1. Properties of the crude oils from which the n-C_7 insolubles were obtained.

Property	CH-02	RB-1319	PG-49	AR-4
Oil Gravity (°API)	9.4	12.76	13.6	29.8
TAN (mg KOH/g oil)	<0.10	0.53	5.7	0.11
Asphaltenes 96h (%)	8.7	7.2	0.61	1.1

Table 2 contains the elemental composition for each n-C_7 insoluble extract, where sulphur seemed the most variable element in all the samples. While CH-02 had 5.15%, AR-4, just 0.91%. Regarding the H/C, PG-49 had the highest ratio 1.18, and RB-1319 the lowest, 0.87. This could be related with the architecture of asphaltenes considering that island-type structures use to have more carbon than hydrogen, but archipelago-type asphaltenes have more hydrogen due to a high concentration of alkyl chain bridges between aromatic nuclei.

Table 2. Elemental composition for the n-C_7 insolubles under study

Asphaltenes	%C	%H	%N	%S	%O*	H/C
CH-02	82.56	7.41	1.7	5.15	3.18	1.07
RB-1319	87.3	6.3	1.41	3.2	1.79	0.87
PG-49	81.19	8	1.83	2.53	6.45	1.18
AR-4	85.9	7.22	0.88	0.91	5.09	1.02

ASPHALTENE OXIDATION REACTIONS

Two oxidizing reactions conditions were developed on four fractions precipitated with n-C_7; the first oxidation consisted of the reaction with a mixture of acetic acid and hydrogen peroxide at 20 °C (O1) and the second one, the oxidation was carried out to 60 °C (O_2). After reaction completion, the products were isolated following the procedure described in the experimental section. The amount of raw n-C_7 insolubles was 50 mg, and yields were calculated (Table 3) based on starting material as solid yield (mg of oxidized n-C_7 insolubles/50 mg of starting material * 100). In some cases, the weight of the products was less than the initial mass, hence a solid yield lower than 100 % was obtained. This can be understood considering that part of the products is water soluble and, therefore, discarded during the reaction workup.

Table 3. Reaction solid yields under oxidation conditions

Asphaltenes	Yield (%)			
	CH02	RB1319	PG49	AR4
O1	80	97.68	83.2	94.2
O2	68	101.2	87.6	96.6

*O1: 50 mg of asphaltenes, AcOH (103 µL), H_2O_2 (µL), DCM, r.t. O_2: 50 mg of asphaltenes, AcOH (103 µL), H_2O_2 (µL), toluene, 60 °C.

Under both oxidation conditions (O1 and O_2), the lowest solid yield was observed for CHO_2 followed by PG49. These implies that part of the products obtained by CHO_2 oxidation were water soluble. On the other hand, the highest yield was reached for RB1319, where nearly non water soluble products were obtained. Both results could be associated with the structure of the starting molecules. Under oxidative conditions, archipelago type molecules would undergo C-C bond cleavage along their CH_2 bridges and generate water-soluble oxidized fragments (low molecular weight structures), which would provide a relatively lower solid yield. On the other hand, island-type molecules would not suffer such cleavage, and thus the oxygen atoms incorporated might remain on the aromatic nuclei (increasing their molecular weight) (Maddams, 1980), generating molecules that are non-water-soluble, and so obtaining a relatively higher mass yield (even above 100 %). Based on this reasoning, a first classification of the samples according to the prevalence of archipelago/island molecules would be CHO_2 > PG49 > AR4 and > RB1319. This corresponds to the increasing order of reaction yield for both oxidation conditions. However, these outcomes must be corroborated with the FTIR characterization, as it will be further discussed.

INFRARED CHARACTERIZATION OF ASPHALTENE AND THEIR OXIDATION PRODUCTS

The spectra profiles resembled heavy oil fractions (Figure 2). Broadly, this type of spectra show aliphatic moieties around 3000-2750 and 1450-1350 cm^{-1}, aromatic groups around 3050, 1600 and 900-700 cm^{-1}, carbonyl ones between 1750 and 1650 cm^{-1}, sulfones at 1100 900 cm^{-1}, and other functionalities in the fingerprint region (1100-1350 cm^{-1}). Since all spectra were normalized, vibration bands should be understood as relative abundances of the functional groups assigned. Nevertheless, the quantification of functional groups by IR is limited when using ATR. In this case, the amount of irradiated sample is a function of the depth of penetration of the IR radiation, which in turn depends on the refractive index of the material and the wavelength. However, it is relatively common to propose relationships between intensities. Whatever the absorptivity values are for two different functional groups, the absorptivity ratio will remain constant. Thus, if the intensity of one of them changes, said change can be associated with the process to which the sample has been subjected (Orrego-Ruiz, et al., 2015; Orrego-Ruiz, et al., 2022; Orrego-Ruiz, et al, 2011)

It is worth to note that independently of the fraction precipitated with n-C_7 and the reaction condition (O1 and O_2) employed, the carbonyl (1800-1600 cm^{-1}) and sulfone (1100-900 cm^{-1}) groups increased with oxidation (Figure 2), as well as the band around 1240-1200 cm^{-1}, ascribable to C-O bond in esters. However, each of these regions will be explored in more detail below.

ALIPHATIC MOIETIES IN REGION 3000-2850 cm^{-1}

Five vibrational bands represent the aliphatic groups -CH_3, -CH_2, and -CH, since both -CH_3 and -CH_2 groups have asymmetric and symmetric vibrational modes, one of their modes (not both) was consider for studying the samples oxidation (Figure 3). In our case, the asymmetric CH_3 (2954 cm^{-1}) (Figure 3a) and symmetric -CH_2 (2850 cm^{-1}) (Figure 3b) bands were chosen to follow the progress of the reaction, considering that they have low overlap with other signals in the deconvolution (Figure 4).

Likewise, the contribution of CH_3 and -CH_2 groups, as well as the ratio CH_2/CH_3 were studied (Figure 3c). Broadly, the relative abundance of -CH_3 decreases throughout the oxidation of n-C_7 insolubles (Figure 3a), except in RB1319, where both reaction conditions triggered a relative increasing in -CH_3 groups. Methyl groups are interesting moieties to track the position of alkyl topologies on n-C_7 insolubles structures throughout oxidation reactions, since oxidation is more suitable on α-H of side alkyl chains (Vetrivel, & Pandurangan 2004). Hence, it is expected that CHO_2, AR4 and PG49 have more benzylic -CH_3 moieties available to react than RB1319 (Figure 3a). Such functional groups were further oxidized in PG49 and AR4 under more drastic conditions (O_2), since the area of CH_3 decreased under O_2 conditions. In the case of CHO_2, benzylic -CH_3 groups decrease their concentration under O1 conditions, but with O_2 conditions (more time and temperature) the -CH_2 oxidations on non-alpha positions seem to be viable (A Pandurangan, 2004), since -CH_2 decreases importantly, but -CH_3 seemed almost constant. Then, the oxidation of methylene groups would allow preserving terminal alkyl chains that imply a relative increase in the concentration of -CH_3 and a decrease in CH_2 (Figure 3b). Accordingly, CHO_2 correspond to a fraction precipitated with n-C_7 enriched in alkyl bridges linking aromatic nuclei that at higher temperatures (60 °C) suffer cleavage, incorporate oxygen in their resulting cores, and loss mass by the dissolution of such highly

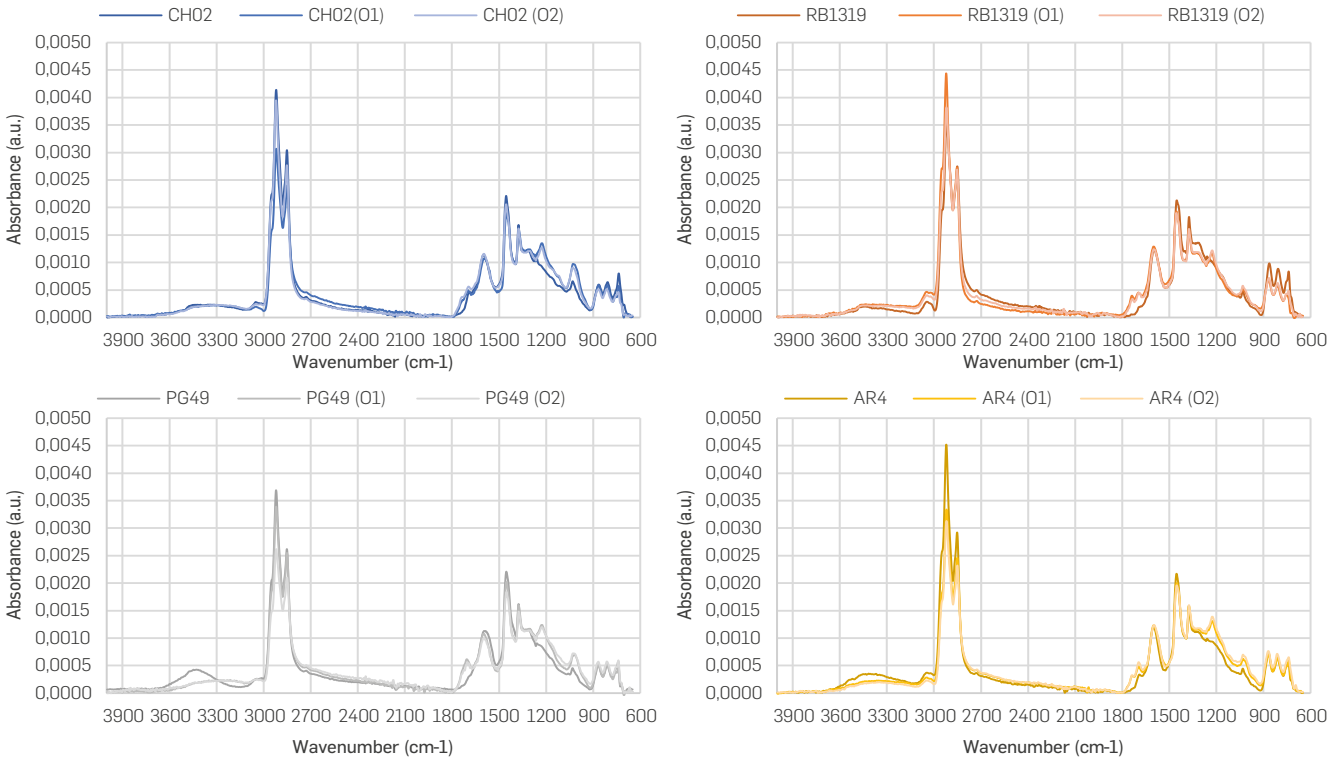

Figure 2. FTIR profiles for asphaltenes and their oxidized products

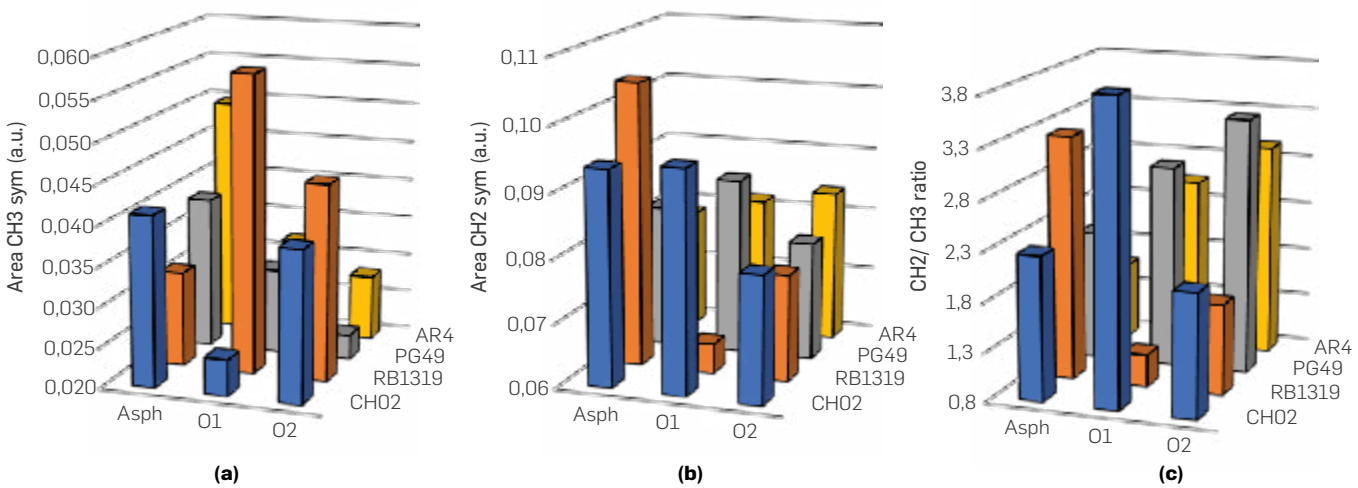

Figure 3. Variation of aliphatic groups for n-C_7 insolubles and oxidation products a) -CH_3, b) -CH_2 and c) CH_2/CH_3 ratio

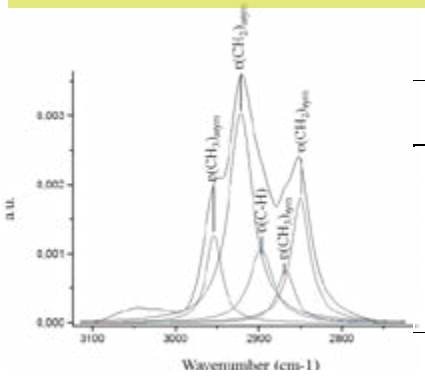

Assignation	Wavenumber (cm^{-1})	CH02			RB1319			PG49			AR4		
		Asph	O1	O4	Asph	O1	O4	Asph	O1	O4	Asph	O1	O4
$n(CH_3)_{asym}$	2954	0.0414	0.0246	0.0389	0.0319	0.0572	0.0445	0.0390	0.0307	0.0232	0.0496	0.0321	0.0283
$n(CH_2)_{asym}$	2923	0.1685	0.1179	0.1611	0.1405	0.1974	0.1665	0.1552	0.1298	0.0955	0.1941	0.1345	0.1257
n(C-H)	2898	0.0682	0.0538	0.0590	0.0666	0.0505	0.0569	0.0552	0.0555	0.0453	0.0582	0.0516	0.0491
$n(CH_3)_{sym}$	2868	0.0299	0.0124	0.0278	0.0202	0.0360	0.0304	0.0225	0.0183	0.0132	0.0342	0.0210	0.0159
$n(CH_2)_{sym}$	2850	0.0936	0.0946	0.0799	0.1043	0.0646	0.0767	0.0823	0.0876	0.0786	0.0787	0.0816	0.0838

Figure 4. Deconvolution of region 3000-2750 cm^{-1}

oxygenated moieties in water. The lastter is in accordance with the yields presented in Table 3, where under O_2 conditions CHO_2 rendered the lowest reaction yield.

Regarding -CH_2, the changes were less severe compared to -CH_3 and there was not a defined tendency along the oxidation (Figure 3b). For CHO_2 and PG49 there was a relative increase on methylene groups under O1 conditions and a relative decrease using O_2 conditions. AR4 slightly increased in CH_2 along the reactions, while RB1319 decreased drastically such moieties. This allows inferring that n-C_7 insolubles RB1319 are enriched in methylene groups attached to aromatic cores where the two alpha carbons represent a higher reactivity compared to an aliphatic chain bonded to a ring [39,47 This would suggest the prevalence of naphthenic groups in RB1319. Thus, RB1319 is oxidized over its methylene groups by means of HOO· radicals, affording different oxidated groups (Shabalin, et al., 2020). These statements will be later correlated with other functional groups. The degradation of such naphthenic cores generates ring opening reactions and hence new -CH_3 groups, as it was detected for these n-C_7 insolubles (Figure 3a). The changes found in CH_2/CH_3 ratio (Figure 3c) help to reinforce that the oxidation over AR4 and PG49 leads preferentially to the loss of benzylic -CH_3 groups, since the ratio CH_2/CH_3 increased for these n-C_7 insolubles. Furthermore, higher values in CH_2 under O1 conditions for CHO_2, PG49 and AR4 can evidence that kinetic control is more prone over CH_3 than CH_2 groups under O1 oxidation conditions.

Regarding O_2 conditions, this ratio is governed by thermodynamic control, where oxidative agents combined with heating goes for -CH_2 groups, starting with the benzylic ones. In sum, based on these outcomes, the reactivity order for n-C_7 insolubles' aliphatic chains is CH_3-Benzylic > CH_2-Benzylic > CH_2. Since AR4 slightly increased in -CH_2, this would mean that such methylene groups are not affected by oxidation because they are part of long alkyl chains (acyclic). Thus, such increasing might be understood as a relative change, if it is considered that a marked decrease in methylene groups should be due the oxidation of benzylic moieties. The areas obtained by deconvolution of region 1800-1600 cm^{-1} are presented in Table S2. This region, that includes carbonyl groups that form part of aldehydes, ketones, esters, acids and/or anhydrides, as well as aromatic carbons, is important due to the high specificity that can be reached for oxygenated compounds. This can be acknowledged as an advantage for IR over other techniques, since thanks to the high sensitivity in the detection of carbon–oxygen vibrations, which have high absorptivity in the infrared spectrum, it is possible to detect and distinguish these functional groups that usually are hardly detected by NMR (Sánchez & de Klerk, 2016b). Figure 5 presents the areas of bands deconvoluted in region 1800-1600 cm^{-1}, corresponding to carbonyl groups for the starting n-C_7 insolubles and their oxidation products.

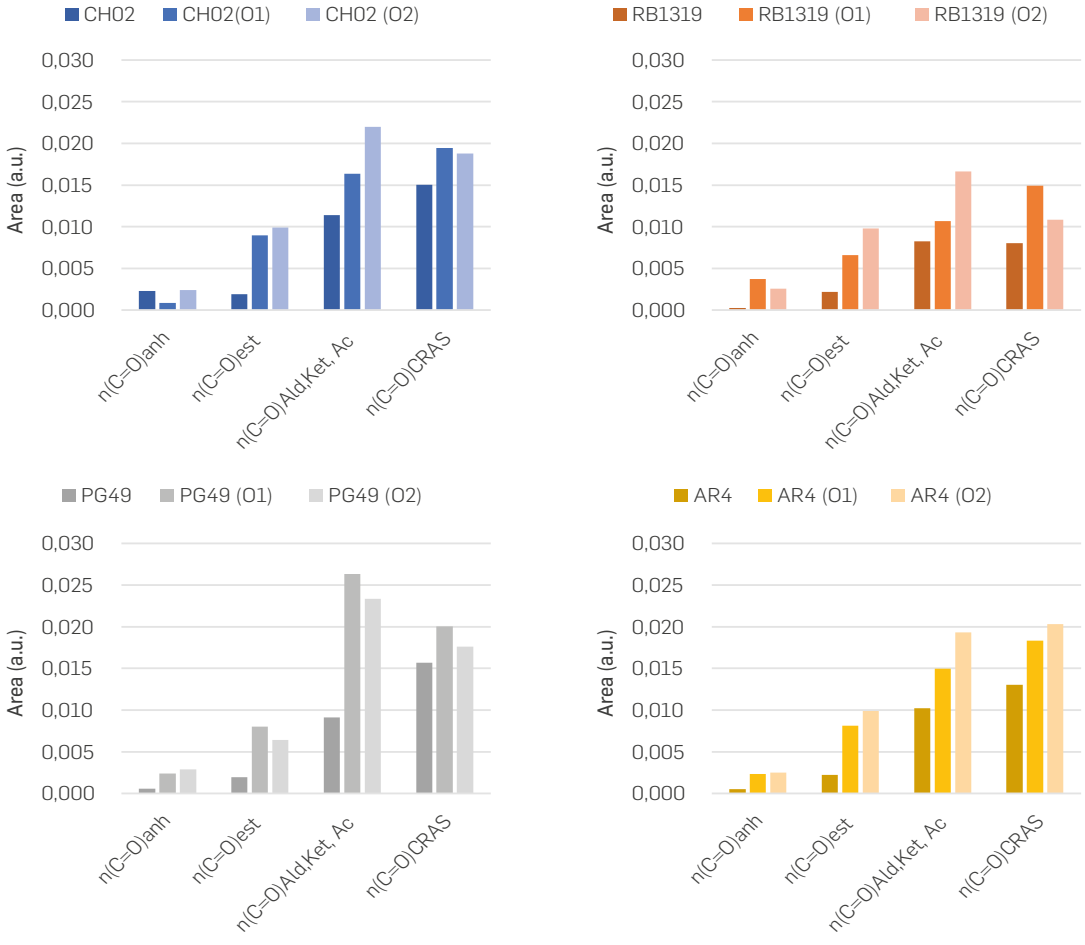

Figure 5. Variation of oxygenated compounds (region 1800-1600 cm^{-1}) along the oxidation

CARBONYL MOIETIES IN REGION 1700-1730 cm^{-1}

Broadly, all the carbonyl groups increased their concentration along the oxidation of n-C_7 insolubles in the order of O1 < O_2, as was mentioned earlier. Nevertheless, considering the increasing of the areas from asphaltene towards oxidation products for all the samples (more than double in all cases), the esters were one of the main functional groups generated during oxidation. Thus, the changes observed for esters were worth to be examined in detail, since apart from the C=O bond around 1730 cm 1, the C-O band can be detected within the fingerprint region (Zojaji et al., 2021). In other words, although the fingerprint region was not deconvoluted, the intensity around 1240 cm^{-1} was associated to the CO ester bond. Thus, for each sample the intensity of this band was correlated with the area of the band υ(C=O)est at 1730 cm^{-1}(see Table S2). Figure 6 shows the parity plot for these two parameters.

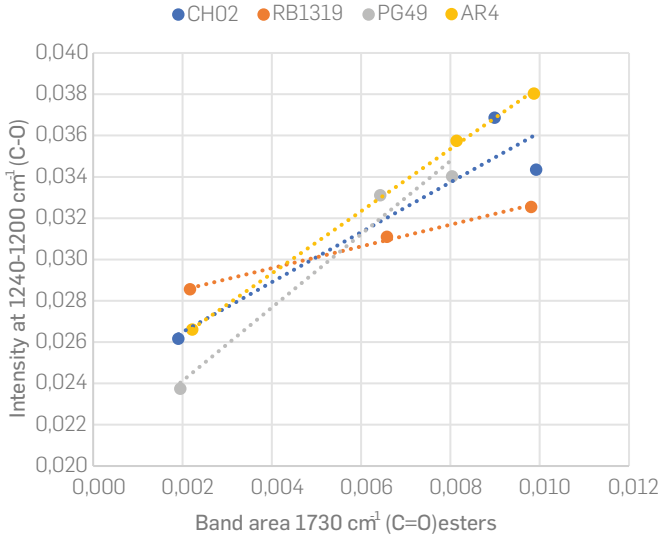

Figure 6. Parity plot for the band area C=O (1730 cm^{-1}) and intensity C-O (1240 cm^{-1})

A positive correlation with R2 0.85 was an indicator that both signals are related, and hence a confirmation of esterification along the course of oxidation reactions. Interestingly, the slope was different for each group of samples. The highest were found for PG49 and AR4, while the lowest was for RB1319. This could be associated with a higher formation of cyclic esters (lactones) over linear esters, since the formation of such groups on aromatic cores may imply a higher intensity for the band around 1230 cm^{-1}. For instance, considering the IR spectrum of an aromatic lactone such as the 3,4 dihydrocoumarin, the intensity at 1230 cm^{-1} is comparable with the carbonyl group around 1760 cm^{-1}. However, for methyl stearate (an aliphatic ester), the intensity of the band around 1230 cm^{-1} has half the intensity of the band around 1740 cm^{-1}, as it can be verified at the AIST Spectral Database for Organic Compounds (AIST, 2021) Asemani. This implies that the formation of lactone moieties on aromatic nuclei can correspond to a higher slope in a parity plot of the intensities of these two bands (1730 cm^{-1} and 1230 cm^{-1}).

The formation of such esters/lactones (υ(C=O)est) was reported during the reaction of polycyclic aromatic hydrocarbons under oxidative conditions (Martín-Martínez, et al., 2015; Giri & Chauhan, 2009). These groups can be formed by means of a double bond oxidation with ring opening followed by an intramolecular esterification/dehydration (Scheme 1a) (Giri & Chauhan, 2009) (Golchoubian & Hosseinpoor 2007) and/or throughout a benzyl group reacting with a hydroperoxyl radical (HOO•) via cycloalkane autoxidation, as proposed by Montoya and de Klerk (Sánchez & de Klerk, 2016b) (Scheme 1b).

AROMATIC SYSTEMS IN REGION 1600 cm^{-1}

According to Clar's rule, for the same number of aromatic rings, cata-condensed nuclei have a greater number of fixed double bonds compared to a peri-condensed nuclei (Martín-Martínez et al., 2015). Figure 7 shows the differences in cata- and peri-condensed systems, where the γ(CAr-H) 4H hydrogen atoms were coloured in red, γ(CAr-H) 3H in green, γ(CAr H) 2H in black, and γ(CAr-H)¹H in purple. Since the carbon atoms involved in such fixed double bonds are expected to be reactive centres, a cata condensed nuclei should

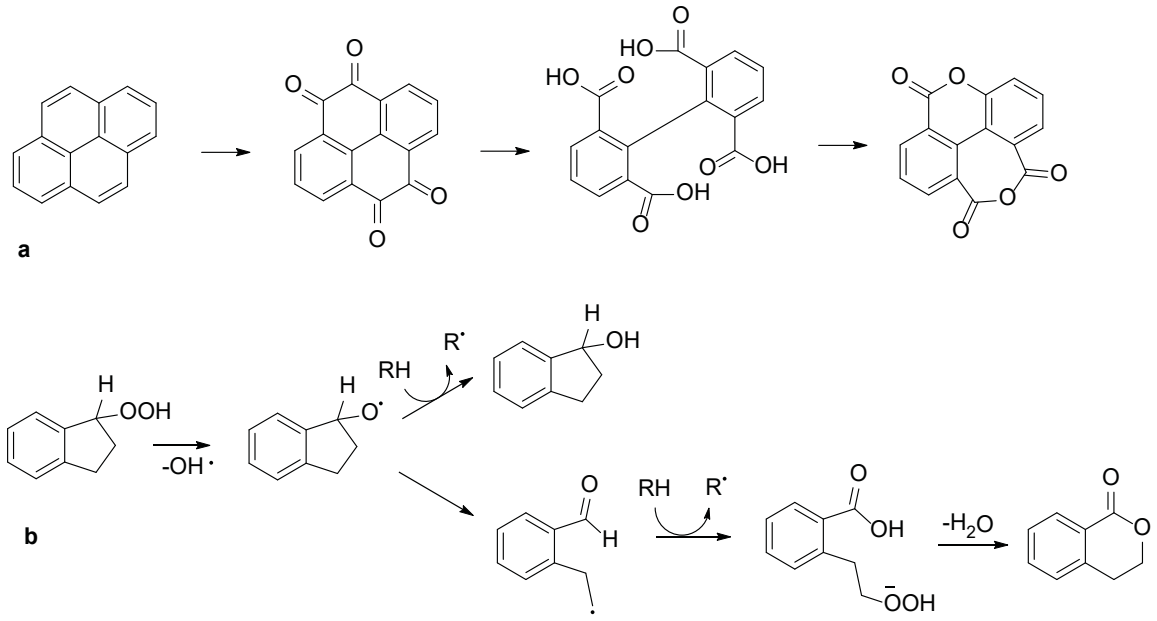

Scheme 1. Lactone formation: a. Proposed decarboxylation and intramolecular condensation reactions; b. Reaction pathway of ester-lactone formation via oxidation-ring opening-condensation (Adapted from: Appl Petrochem Res (2016) 6:97–106)

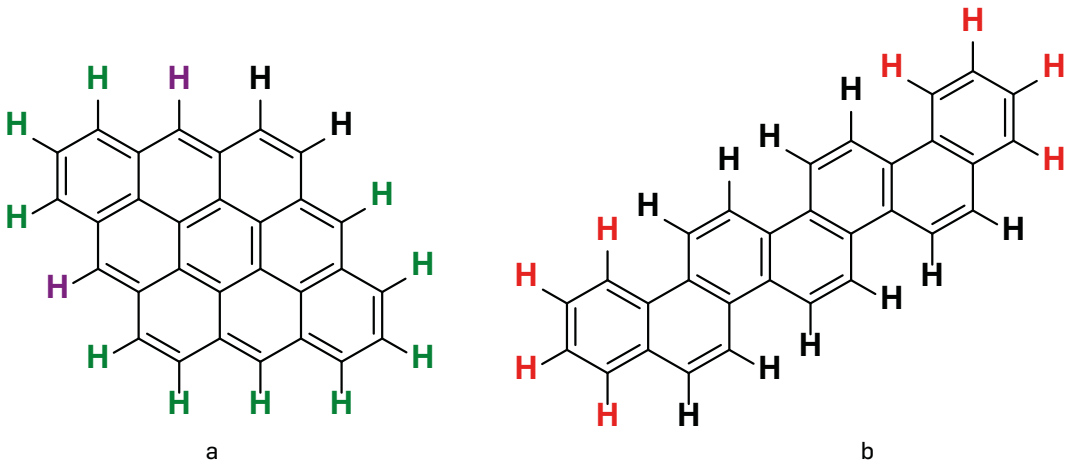

Figure 7. Peri and cata-condensed structures type. a) Systems with 1, 2 or 3H associated with peri condensed or highly substituted rings, b) Systems rich in 4 and 5H represented by cata-condensed structure

exhibit greater reactivity than a peri condensed nuclei towards the oxidation of aromatic cores in intramolecular condensation reactions (scheme 1a) implying the formation of lactones. Namely, cata-condensed asphaltenes would have a greater tendency to generate esters, anhydrides, or ketones on the aromatic cores. Based on these outcomes, PG49 > AR4 > CHO_2 > RB1319 can be proposed as a decreasing order for cata-condensed prevalence of asphaltenes nuclei, which coincides with the decreasing order for the slopes displayed in Figure 6.

Nevertheless, similar oxidative conditions have shown that peri-condensed polycyclic hydrocarbons such as benz[a]anthracene affords a less complex mixture of products with a lower degree of oxidation (phenol, ketone), while cata-condensed systems such as pyrene can afford a more complex mixture of compounds with a higher oxidation degree (ketones, di-acids, anhydrides, etc) that can be convened as carbonylic-rich alicyclic systems (CRAS) (Giri & Chauhan, 2009). These last ones must imply the ring opening and intramolecular condensation/dehydration processes mentioned above (Scheme 1a), yielding aromatic anhydrides. Such reactions can be considered an increase in anhydride species with decreasing CRAS as it was observed for n-C_7 insolubles CHO_2 and PG49 (Figure 5). The formation of esters, anhydrides, or ketones on the aromatic cores ($C{=}O_Q$) all might imply a loss of aromaticity, as it will be discussed below. On the other hand, PG49 increased carbonyl systems (carboxylic acids) more than other samples, but under O_2 conditions these changes were slightly less in comparison with O1. This result could be associated to decarboxylation reactions (CO_2 loss) and/or intramolecular condensation reactions (lactones and anhydrides formation via ester condensation and dehydration) prompted by the temperature increase (Ling et al 1999).

Aromaticity was monitored through the area of the band around 1600 cm^{-1}, also obtained from the deconvolution of the 1800-1600 cm^{-1} region. Figure 8 shows the intensities of band $\upsilon C{=}C_{Ar}$ describing the variation on aromaticity for all samples. Even though the changes detected are subtle, some tendencies were found. Aromaticity -seen as the area of the $C{=}C_{Ar}$ band- decreased under O1 conditions for PG49 and CHO_2, increased for RB1319, and had no changes for AR4. Since no alkyl cleavages are expected for island dominant asphaltenes, and the aromaticity of archipelago-dominant asphaltenes should decrease throughout oxidation, when these cleavages occur on the aliphatic bridges connecting the aromatic nuclei. It is possible to state that PG49 and CHO_2 resemble archipelago-dominant n-C_7 insolubles while n-C_7 insolubles AR4 fits better with island dominant structures, since their aromaticity changes are not appreciable according to this parameter. On the other hand, oxidative dehydrogenation of naphthenic frameworks can increase asphaltenes aromaticity. Considering that hydrogen is lost during oxidation as water and can be either due to carbonyl or olefin formation (Siddiquee & De Klerk, 2014). Such naphthene systems dehydrogenation can be noticed as asphaltenes aromaticity growth via FTIR, as occurred with RB1319. The study of conjugated dehydrogenation of naphthene hydrocarbons with hydrogen peroxide that have been reported 46 In this reaction HOO• radicals become the main active sites for the substrate's radicals transformation and occurs through a mechanism different from that for the high-temperature homogeneous oxidation of hydrocarbons by molecular oxygen (Nagiev, 2007b, 2007a) According to these statements, n-C_7 insolubles RB1319 respond to island-dominant structure enriched in naphthenic frameworks. However, it should be mentioned that since HOO• radicals are produced by H_2O_2 vapor dissociation, oxidative dehydrogenation reactions mostly proceed at relatively high temperatures (Nagiev, 2007b; Siddiquee & De Klerk, 2014).

SULPHUR CONTAINING SYSTEMS 700-900 cm^{-1} AND 1000-1040 cm^{-1}

The third and fourth infrared regions considered in this study were 1040-1000 cm^{-1} and 900 700 cm^{-1}. The areas of these bands are compiled in Table S3. Even though four different bands fit within the 1040-1000 cm^{-1} region, all of them were summed and assumed as S=O groups without any discrimination (Figure 9).

According to Figure 9, the S=O groups increased along the oxidation in all n-C_7 insolubles. However, the sulphur containing compounds present in CHO_2 were comparatively more reactive, considering that the increase on S=O area was about twice, changing from 0.010 to 0.021 under O1 conditions, and 0.018 with O_2 conditions. This observation can be interpreted as a major content of sulphide and thioether moieties within CHO_2 asphaltenes, since the rate constants for the oxidation of thiophene derivatives are 2 to 4 orders of magnitude smaller than those for the oxidation of aliphatic sulphides (Brown & Espenson, 1996) and these reaction rates can be approximately 10 fold lower than those of aromatic thioethers such as thioanisole (Nikodinovic-Runic et., 2013) Considering the previous

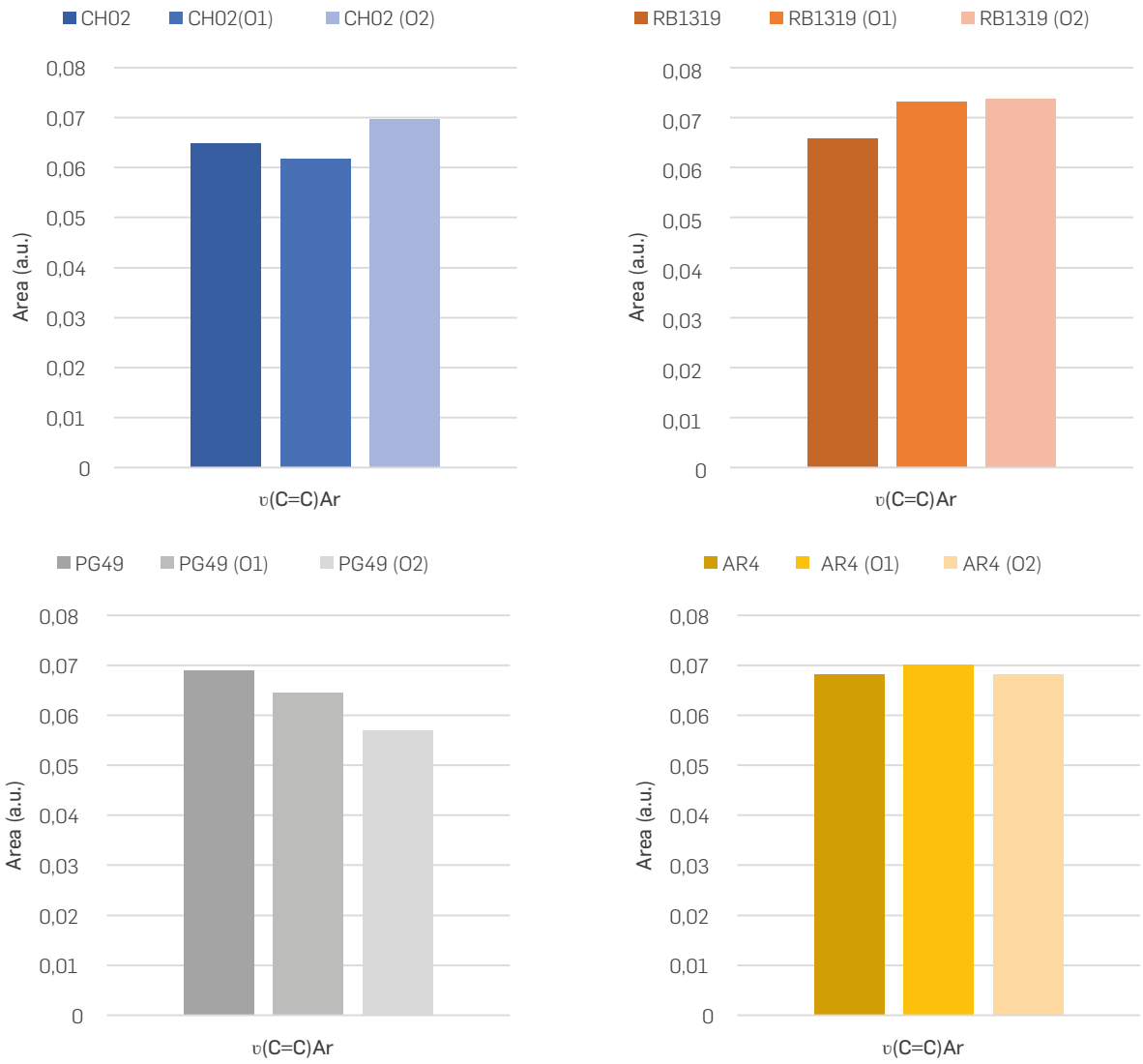

Figure 8. Aromaticity variations seen as the area of the C=Car 1600 cm^{-1} band

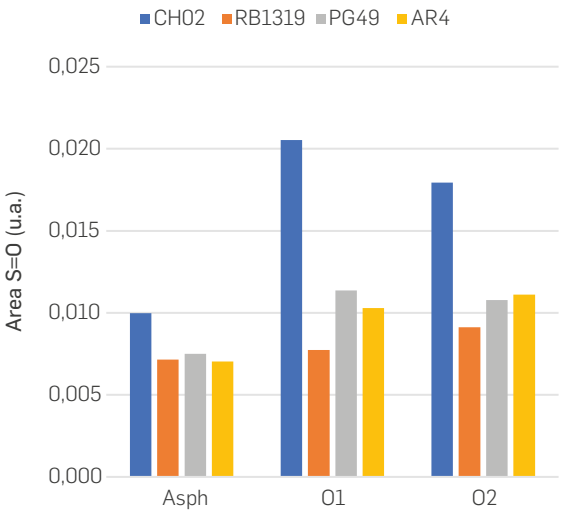

Figure 9. Aromaticity variations seen as the area of the C=Car 1600 cm^{-1} band

facts, RB1319 were the least reactive n-C_7 insolubles regarding the incorporation of oxygen in n-C_7 insolubles as oxysulphur containing compounds. It can be inferred that such sulphur atoms could be present as thiophene structures and, hence hindering the oxidation of sulphur atoms within the asphaltenes structure. Although the oxidation of sulphides and thiophenes to sulphoxides (sulphones and sultones) are usually prompt under transition-metal-catalysed conditions, the oxidation of such compounds using hydrogen peroxide and glacial acetic acid without catalyst have been reported, as well (Golchoubian & Hosseinpoor, (2007) ; Kaczorowska, et al., 2005)

Regarding the aromatic groups detected in 900-700 cm^{-1}, trends were not easily tracked. The areas corresponding to these bands are compiled in Table S3. The γ(C_{Ar} H) ^{1}H corresponds to hydrogens linked to penta-substituted aromatic rings, hydrogen atoms that form part of aromatic rings where five of the six carbon atoms do not have hydrogens attached and are hence considered a highly-condensed system. On the other hand, the γ(CAr-H) 2H,3H, γ(C_{Ar}-H) 4H and γ(C_{Ar}-H) 5H represent structures where 2-3, 4 and 5 hydrogens are neighbours. These last two bands represent aromatic systems where up to five of the six carbon atoms are substituted. Therefore, these bands can be assumed as indicators

of the substitution degree of the periphery of the aromatic rings conforming the asphaltenes' nuclei. In this sense, systems enriched in 1, 2 or 3H could be associated to either peri condensed or highly substituted rings, as shown in Figure 7a, while systems enriched in 4 and 5H could be better represented by a cata-condensed structure or low substituted rings (Figure 7b). Aromatic systems with low substitutions offer a higher probability to incorporate oxygen through addition reactions over the asphaltenes' structures, regardless the prevalence of cata- or peri condensed nuclei. Moreover, according to Scheme 1a, if this oxidation occurs over such double bonds, the signals $\gamma(C_{Ar}\text{-}H)2H,3H$ and $\gamma(C_{Ar}\text{-}H)4H$ should decrease. Bearing this in mind, the sum of these formed carbonylic signals (C=O total; 1800 1600 cm^{-1}) was correlated with the summatory of the bands $\gamma(C_{Ar}\text{-}H)4H$, $\gamma(C_{Ar}\text{-}H)5H$ (Figure 10). According to these results, for CHO_2 and RB1319, the intensity of the signals related to these two groups of hydrogen atoms decrease with the oxidation, which can be ascribable to a low substitution over these asphaltenes' nuclei. Conversely, for AR4 and PG49, the same groups increased slightly. As it was discussed earlier, the formation of esters, anhydrides, or ketones on the aromatic cores ($C=O_Q$) might suggest a loss of aromaticity. Thus, it would imply that on CHO_2 and RB1319 the oxidation occurs mostly over their aromatic cores. Meanwhile, for AR4 and PG49 the oxidation occurs on alkyl groups present, i.e., in the periphery of the aromatic cores, generating carboxylic acids, as particularly observed for PG49 (Figure 5).

ASPHALTENE STRUCTURE APPROACHING.

Based on the above statements, and supported on structural parameters extracted from infrared analysis, some structural descriptors (SD) were proposed. Table 4 lists the main characteristics of the raw n-C_7 insolubles that can give insights for further spectra to structure relationship and/or molecular dynamics studies.

A first approach on the reconstruction of a crude oil using structural descriptors and molecular dynamics have been recently reported (Moncayo-Riascos et al., 2022). Nevertheless, advocating our recent results obtained in the state of the art (Ramírez-Pradilla et al., 2024), as a complementary part of this work, additional hints on the structural domains of these asphaltenes were addressed by thermo oxidative reactions using the TGA MS and ^{1}H NMR experiments.

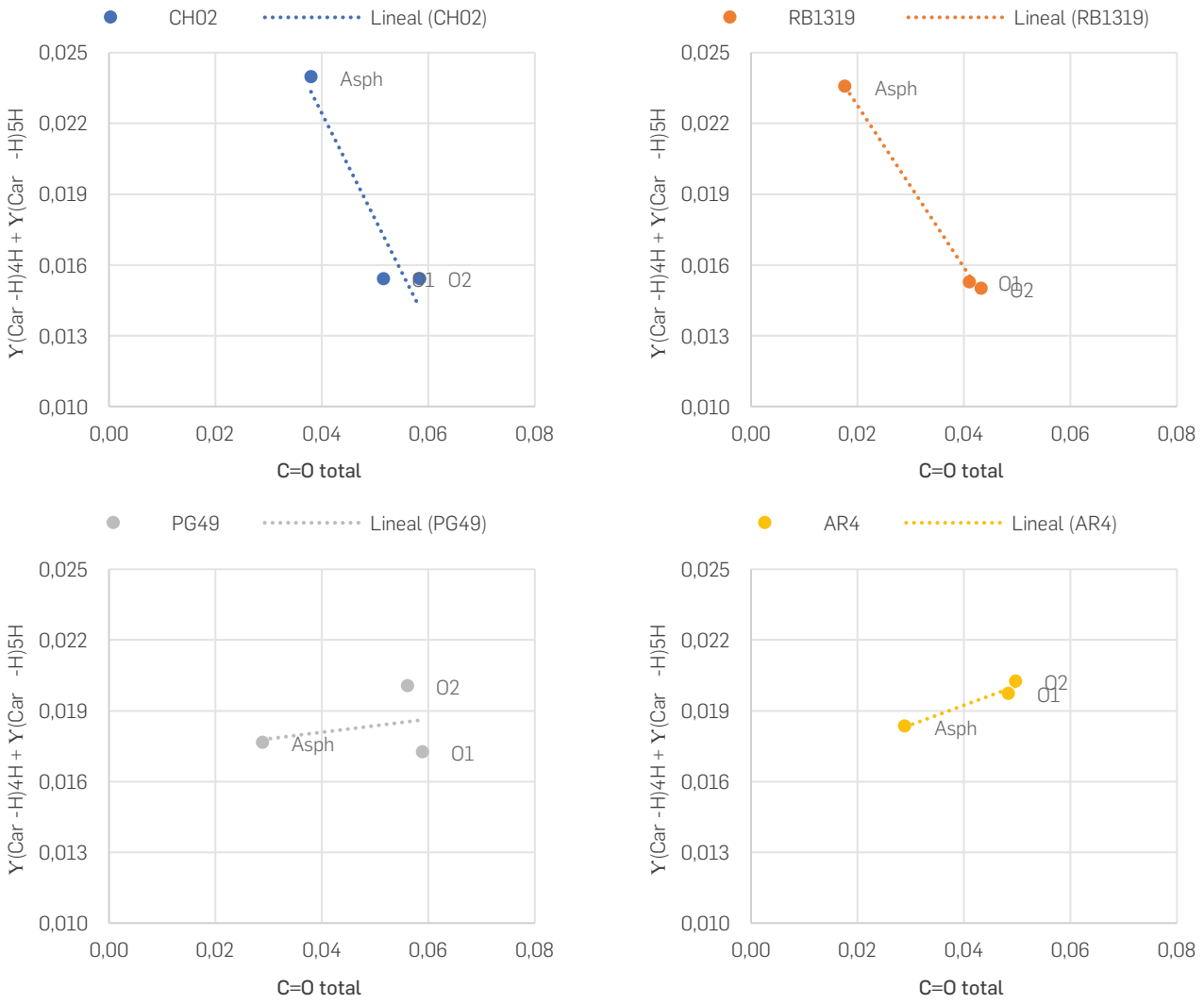

Figure 10. Parity plots of sum of areas γ(CAr-H)4H, γ(CAr-H)5H and total area of carbonylic groups

Table 4. Structural descriptors (SD) based on infrared compositional parameters.

Asphaltene	Asphaltene structural changes after reactions													
	Yield		$-CH_3$ abundance		$-CH_2-$ abundance		Slope C=O vs C-O esters		Aromaticity		S=O abundance		Slope C=O total Vs 4H, 5H	
	Table 2		Figure 3a		Figure 3b		Figure 5		Figure 7		Figure 8		Figure 9	
CH02	Oxidation	SD	Oxidation	SD	Oxidation	SD	Oxidation	SD	Oxidation	SD	Oxidation	SD	Oxidation	SD
CH02	Below 100%	Prevalence of archipelago structures	D	Presence of some benzylic aliphatic carbons	D	Presence of alkyl bridges	M	Presence of Cata condensed nuclei	NT	--	HI	H input of sulfidic entities	D	HS aromatic core
RB1319	Around 100%	Prevalence of island structures	I	Almost none-benzylic groups	HD	Prevalence of naphthenic moieties	L	Prevalence of peri condensed nuclei	I	Prevalence of island structures and/or naphthenic moieties	LI	L input of sulfidic entities	D	HS aromatic core
PG49	Below 100%	Prevalence of archipelago structures	HD	Prevalence of benzylic aliphatic carbons	NT	--	H	Prevalence of Cata condensed nuclei	D	Prevalence of archipelago structures	I	M input of sulfidic entities	NT	--
AR4	Around 100%	Prevalence of island structures	HD	Prevalence of benzylic aliphatic carbons	I	Prevalence of alkyl moieties	H	Prevalence of Cata condensed nuclei	NT	--	I	M input of sulfidic entities	I	LS aromatic core

L: Low, M: Medium, H: high, S: Substituted, I: increasing, D: Decreasing, NT: no tendency, Ox: Oxidation

REACTIVITY UNDER THERMO-OXIDATIVE CONDITIONS: THERMOGRAVIMETRIC ANALYSIS COUPLED TO MS EXPERIMENTS.

The thermogravimetry using an oxidizing atmosphere offers valuable information about the reactivity behaviour of each asphaltenes towards the oxygen molecule. Under the conditions proposed in this work, noticeable differences were observed on the combustion profiles for each asphaltene, spanning from highly reactive at low temperature, to oxidizing-resistant samples. According to the experimental set-up, the thermogravimetric analysis was performed while the produced gases were analyzed by low resolution mass spectrometry using a quadrupole analyzer in function of time. This approach allowed linking the weight loss of the samples with the CO_2 production during the process. Figure 11 shows both, the mass lost as a function of temperature and time (Figure 9a), as well as the relative abundance (%R.A.) of CO_2 produced during combustion (Figure 10b). It can be observed that asphaltenes PG49 exhibited the greatest weight loss at low temperature, with CO_2 production starting at 14 min (represented around 300 °C) and ending at 28 min. In the case of CHO_2, the weight loss began in longer times (Figure 11a), but the CO_2 production started at the same time of PG49 and, therefore, at the same temperature. However, the CO_2 profile ended in about 36 min, which increased the maximum CO_2 production at higher temperatures. This means that, CHO_2 produced CO_2 in a broader band time in comparison with PG49. This can be explained considering that once the alkyl chains are cleaved, the larger the aromatic core remaining, the greater the amount of energy required for complete oxidation.

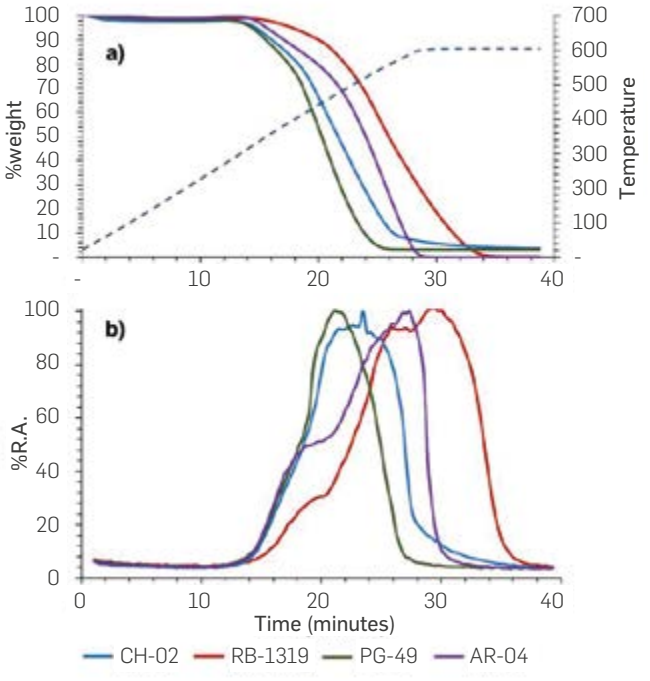

Figure 11. (a) Thermogravimetric analysis of asphaltenes coupled to low-resolution mass spectrometry. (b) MS profile of CO_2 from combustion

The foregoing implies that the aromatic cores present in CHO_2 must be larger than those present in PG49. In other words, these results confirm that CHO_2 corresponds to archipelago peri-condensed dominant asphaltenes, while PG49 are archipelago cata-condensed dominant asphaltenes and/or aromatic cores smaller than CHO_2 (Table 4). Regarding RB1319 and AR4, TGA-MS analysis revealed that weight loss occurred at higher temperatures. For these samples, the loss of 50 % of initial weight occurred at temperatures above 550 °C, while this behaviour was observed at around 450 °C for PG49 and CHO_2 (archipelago-dominant asphaltenes).

^{1}H-NMR ANALYSIS

To support these observations, we performed ^{1}H-NMR experiments (Figure 12), in which we observed that asphaltenes PG49 and CH02 exhibited a higher percentage of hydrogens within the high-field region than RB1319 and AR4. As this proton signals are assigned to methyl (H8) and paraffinic (H7) groups, these two asphaltenes showed higher contribution to the ^{1}H-NMR spectra by their alkyl chains moieties. These observations are meaningful when analyzing the low field region, in which RB1319 and AR4 exhibited the highest abundance of hydrogens (H2 and H3), which corresponds to aromatic units. This confirms the TGA observation where the island asphaltenes RB1319 and AR4 exhibited a higher resistivity to the thermal oxidation, attributed to the contribution of relatively higher aromatic molecules within the asphaltene samples.

Such behaviour can be associated to island-dominant asphaltenes whose structures might resist to the combustion at higher temperatures, and less weight losses are observed. Particularly, for RB1319, the greatest weight loss was observed at the highest temperature of the ramp (600 ° C), which is consistent with the structure proposed via oxidation-FTIR analysis. Furthermore, the CO_2 profile of RB1319 is the broadest, indicating a high resistance to oxidation when compared to all samples and particularly to AR4. These facts indicate that, under the oxidative conditions used during TGA-MS, RB1319 are the least reactive asphaltenes of the series as observed via mild oxidation and FTIR analysis (conditions O1 and O_2). When considering the CO_2 profile for AR4, a shoulder around 16 min and an extended band at 36 min were observed. Such shoulder can be attributed to the early combustion of the alkyl chains attached to the main island-dominant aromatic nuclei. Next, the remaining aromatic nuclei would be converted to CO_2 at higher temperatures (and therefore at higher times). For RB1319, on the other hand, two shoulders at 18 min and 26 min were noticed, and a significant portion of the CO_2 profile was at 600 °C. The first shoulder can be associated to alkyl chains attached to the aromatic cores, while the second one to the combustion of naphthenic moieties bonded to these aromatic cores. In terms of reactivity, it can be concluded that asphaltenes PG49 and CH02 consist in archipelago-dominant structures with a higher reactivity towards oxygen, which allows to associate the behaviour under mild oxidation discussed above and, thus, these asphaltenes turn to be more reactive than asphaltenes AR4 and RB1319, which is consistent with the resistivity against thermal oxidation showed during the experiments (Figure 11).

CONCLUSIONS

Two oxidative reaction conditions were proposed for the characterization of asphaltenes from four crude oils using hydrogen peroxide/glacial acetic acid to study the oxidation products by infrared spectroscopy. The reaction yields suggest the prevalence of archipelago or island-dominant structures, since the molecules with alkyl bridges can undergo cleavage and generate water-soluble products affording low yields in solid product. Although infrared spectroscopy has limited accuracy for quantitative approaches and analysis is performed based on bands intensity ratios, it was possible to trace the oxidation reactions by means of the relative increase on carbonyl and sulfone type compounds, as these functional groups are particularly sensitive in the mid infrared. It was confirmed, accordingly, that methyl groups are useful moieties on tracing the position of alkyl topologies on asphaltenes structures throughout oxidation reactions, since oxidation is more suitable on α-H of side alkyl chains. Hence, the reactivity order on aliphatic chains is CH_3

a)

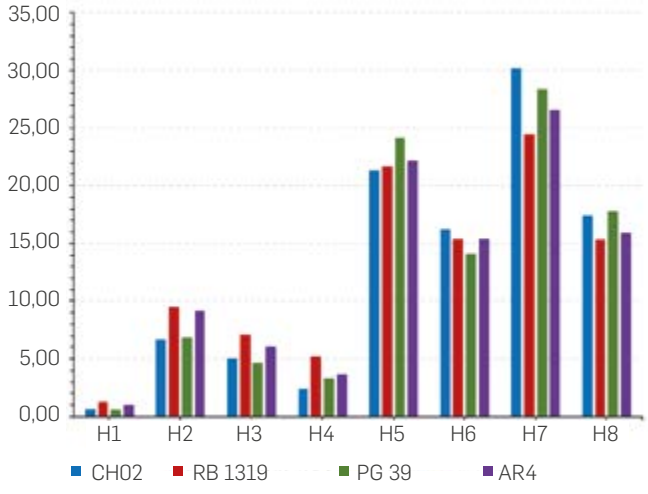

b)

Shift ppm	H_1 12.0 - 9.0	H_2 9.0 - 7.2	H_3 7.2 - 6.0	H_4 6.0 - 4.5	H_5 4.5 - 2.0	H_6 2.0 - 1.5	H_7 1.5 - 1.0	H_8 1.0 - 0.1
Information	Aldehidic and carboxilic acid	Aromatic hydrogen linked to aromatic carbons in polyaromatic rings	Aromatic hydrogen linked to monoaromatic rings	Olefinic hydrogen	Paraffinic and naphtenic hydrogen	Naphtenic hydrogen	Paraffinic hydrogen and alkyl termination	Hydrogen from methyl groups

Figure 12. a) NMR-^{1}H experiments of evaluated asphaltenes and b) Chemical shifts and type of hydrogens of asphaltenes under ^{1}H-NMR experiments

Benzylic > CH_2 Benzylic > CH_2. Considering the increasing of the areas within the region 1800-1600 cm^{-1} for the oxidation products, it was inferred that the esters were the main functional groups formed under the oxidation conditions used. The formation of lactone esters on aromatic nuclei can be monitored through the slope of a parity plot between the intensities of the bands around 1730 cm^{-1} and 1230 cm^{-1}. The prevalence of cata and peri condensed structures can be exanimated by means of monitoring the formation of aromatic esters. Since fixed double bonds are expected to be reactive centers, a catacondensed nuclei should exhibit a greater reactivity than a pericondensed nuclei towards the oxidation of aromatic cores throughout intramolecular condensation reactions. The formation of sulfones during the n-C_7 insoluble oxidation can be related to the prevalence of sulphides and thioethers entities within their structures. Most of the structural features revealed by mild oxidation-FTIR analysis were corroborated by TGA-MS analysis and ^{1}H-NMR.

ACKNOWLEDGEMENTS

The authors would like to thank Ecopetrol S.A. for the funding and authorization for publishing these results.

REFERENCES

AIST. (2021). *Spectral Database for Organic Compounds SDBS.* 3,4-Dihydrocoumarin. https://sdbs.db.aist.go.jp/sdbs/cgi-bin/direct_frame_top.cgi

Asemani, M., & Rabbani, A. R. (2020). Detailed FTIR spectroscopy characterization of crude oil extracted asphaltenes: Curve resolve of overlapping bands. *Journal of Petroleum Science and Engineering,* 185, 106618. https://doi.org/10.1016/j.petrol.2019.106618

Bian, H., Kan, A., Yao, Z., Duan, Z., Zhang, H., Zhang, S., Zhu, L., & Xia, D. (2019). Impact of Functional Group Methylation on the Disaggregation Trend of Asphaltene: A Combined Experimental and Theoretical Study. *The Journal of Physical Chemistry C,* 123(49), 29543–29555. https://doi.org/10.1021/acs.jpcc.9b07695

Brown, K. N., & Espenson, J. H. (1996). Stepwise oxidation of thiophene and its derivatives by hydrogen peroxide catalyzed by methyltrioxorhenium (VII). *Inorganic chemistry,* 35(25), 7211-7216. https://doi.org/10.1021/ic960607+

Cagniant, D., Nosyrev, I., Cebolla, V., Vela, J., Membrado, L., & Gruber, R. (2001). Structural modifications of petroleum asphaltenes by reductive alkylation investigated by TLC-FID. ***Fuel,*** 80(1), 107–115. https://doi.org/10.1016/S0016-2361(00)00041-7

Chacón-Patiño, M. L., Rowland, S. M., & Rodgers, R. P. (2018). Advances in Asphaltene Petroleomics. Part 3. Dominance of Island or Archipelago Structural Motif Is Sample Dependent. ***Energy and Fuels,*** 32(9), 9106–9120. https://doi.org/10.1021/acs.energyfuels.8b01765

Chacón-Patiño, M. L., Niles, S. F., Marshall, A. G., Hendrickson, C. L., & Rodgers, R. P. (2020). Role of molecular structure in the production of water-soluble species by photo-oxidation of petroleum. *Environmental Science and Technology,* 54(16), 9968–9979. https://doi.org/10.1021/acs.est.0c01158

Chacón-Patiño, M. L., Vesga-Martínez, S. J., Blanco-Tirado, C., Orrego-Ruiz, J. A., Gómez-Escudero, A., & Combariza, M. Y. (2016). Exploring Occluded Compounds and Their Interactions with Asphaltene Networks Using High-Resolution Mass Spectrometry. ***Energy and Fuels,*** 30(6), 4550–4561. https://doi.org/10.1021/acs.energyfuels.6b00278

Chacón-Patiño, M. L., Rowland, S. M., & Rodgers, R. P. (2017). Advances in asphaltene petroleomics. part 1: asphaltenes are composed of abundant island and archipelago structural motifs. *Energy & fuels,* 31(12), 13509-13518. https://doi.org/10.1021/acs.energyfuels.7b02873

Derenne, S., & Nguyen Tu, T. T. (2014). Characterizing the molecular structure of organic matter from natural environments: An analytical challenge. *Comptes Rendus - Geoscience,* 346(3–4), 53–63. https://doi.org/10.1016/j.crte.2014.02.005

Desando, M. A., & Ripmeester, J. A. (2002). Chemical derivatization of Athabasca oil sand asphaltene for analysis of hydroxyl and carboxyl groups via nuclear magnetic resonance spectroscopy. ***Fuel***, 81(10), 1305-1319. https://doi.org/10.1016/S0016-2361(02)00040-6

Díaz-Sánchez, H., Rojas-Trigos, J. B., Leyva, C., & Trejo-Zárraga, F. (2017). An approach for determination of asphaltene crystallite by X-ray diffraction analysis: A case of study. *Petroleum Science and Technology,* 35(13), 1415–1420. https://doi.org/10.1080/10916466.2017.1336771

Elbaz, A. M., Gani, A., Hourani, N., Emwas, A. H., Sarathy, S. M., & Roberts, W. L. (2015). TG/DTG, FT-ICR mass spectrometry, and NMR spectroscopy study of heavy fuel oil. *Energy & Fuels,* 29(12), 7825-7835. https://doi.org/10.1021/acs.energyfuels.5b01739

Evstigneyev, E. I., & Shevchenko, S. M. (2019). Structure, chemical reactivity and solubility of lignin: a fresh look. In *Wood Science and Technology* (Vol. 53, Issue 1). Springer Berlin Heidelberg. https://doi.org/10.1007/s00226-018-1059-1

Fakher, S., Ahdaya, M., Elturki, M., & Imqam, A. (2020). Critical review of asphaltene properties and factors impacting its stability in crude oil. *Journal of Petroleum Exploration and Production Technology*, 10(3), 1183–1200. https://doi.org/10.1007/s13202-019-00811-5

Ganeeva, Y. M., Barskaya, E. E., Okhotnikova, E. S., & Yusupova, T. N. (2021). Features of the composition of compounds trapped in asphaltenes of oils and bitumens of the Bavly oil field. *Energy & Fuels*, 35(3), 2493-2505. https://doi.org/10.1021/acs.energyfuels.0c03022

Gargiulo, V., Apicella, B., Alfè, M., Russo, C., Stanzione, F., Tregrossi, A., ... & Ciajolo, A. (2015). Structural characterization of large polycyclic aromatic hydrocarbons. Part 1: The case of coal tar pitch and naphthalene-derived pitch. *Energy & Fuels,* 29(9), 5714-5722. https://doi.org/10.1021/acs.energyfuels.5b01327

Gargiulo, V., Apicella, B., Stanzione, F., Tregrossi, A., Millan, M., Ciajolo, A., & Russo, C. (2016). Structural characterization of large polycyclic aromatic hydrocarbons. Part 2: solvent-separated fractions of coal tar pitch and naphthalene-derived pitch. *Energy & Fuels,* 30(4), 2574-2583. https://doi.org/10.1021/acs.energyfuels.5b02576

Giri, N. G., & Chauhan, S. M. S. (2009). Oxidation of polycyclic aromatic hydrocarbons with hydrogen peroxide catalyzed by Iron (III) porphyrins. *Catalysis Communications,* 10(4), 383-387. https://doi.org/10.1016/j.catcom.2008.09.030

Golchoubian, H., & Hosseinpoor, F. (2007). Effective oxidation of sulfides to sulfoxides with hydrogen peroxide under transition-metal-free conditions. *Molecules,* 12(3), 304-311. https://doi.org/10.3390/12030304

González, G., Sousa, M. A., & Lucas, E. F. (2006). Asphaltenes precipitation from crude oil and hydrocarbon media. *Energy and Fuels,* 20(6), 2544–2551. https://doi.org/10.1021/ef060220j

Hortal, A. R., Hurtado, P., Martínez-Haya, B., & Mullins, O. C. (2007). Molecular-weight distributions of coal and petroleum asphaltenes from laser desorption/ionization experiments. *Energy and Fuels,* 21(5), 2863–2868. https://doi.org/10.1021/ef700225s

Kaczorowska, K., Kolarska, Z., Mitka, K., & Kowalski, P. (2005). Oxidation of sulfides to sulfoxides. Part 2: Oxidation by hydrogen peroxide. *Tetrahedron,* 61(35), 8315-8327. https://doi.org/10.1016/j.tet.2005.05.044

Klein, G. C., Kim, S., Rodgers, R. P., Marshall, A. G., Yen, A., & Asomaning, S. (2006). Mass spectral analysis of asphaltenes. I. Compositional differences between pressure-drop and solvent-drop asphaltenes determined by electrospray ionization Fourier transform ion cyclotron resonance mass spectrometry. *Energy and Fuels,* 20(5), 1965–1972. https://doi.org/10.1021/ef0600199

Klučáková, M., Pelikán, P., Lapčík, L., Lapčíkova, B., Kučerík, J., & Kaláb, M. (2000). Structure and properties of humic and fulvic acids. I. Properties and reactivity of humic acids and fulvic acids. *Journal of Polymer Materials,* 17(4), 337–356. https://www.researchgate.net/publication/259575540_Structure_and_properties_of_humic_and_fulvic_acids_I_Properties_and_reactivity_of_humic_acids_and_fulvic_acids#fullTextFileContent

Kök, M. V., Varfolomeev, M. A., & Nurgaliev, D. K. (2017). Crude oil characterization using tga-dta, tga-ftir and tga-ms techniques. *Journal of Petroleum Science and Engineering,* 154, 537-542. https://doi.org/10.1016/j.petrol.2016.12.018

Kovalenko, E. Y., Gerasimova, N. N., Sagachenko, T. A., Min, R. S., & Patrakov, Y. F. (2020). Characteristics of Products of Thermal Decomposition of Heavy Oil Asphaltenes under Supercritical Conditions. *Energy and Fuels,* 34(8), 9563–9572. https://doi.org/10.1021/acs.energyfuels.0c01796

Liao, Z., Geng, A., Graciaa, A., Creux, P., Chrostowska, A., & Zhang, Y. (2006). Saturated hydrocarbons occluded inside asphaltene structures and their geochemical significance, as exemplified by two Venezuelan oils. *Organic Geochemistry,* 37(3), 291–303. https://doi.org/10.1016/j.orggeochem.2005.10.010

Liao, Z., Zhou, H., Graciaa, A., Chrostowska, A., Creux, P., & Geng, A. (2005). Adsorption/occlusion characteristics of asphaltenes: Some implication for asphaltene structural features. *Energy and Fuels,* 19(1), 180–186. https://doi.org/10.1021/ef049868r

Liotta, R., Rose, K., & Hippo, E. (1981). O-Alkylation Chemistry of Coal and Its Implications for the Chemical and Physical Structure of Coal. *Journal of Organic Chemistry,* 46(2), 277–283. https://doi.org/10.1021/jo00315a010

Llanos, S., Acevedo, S., Cortés, F. B., & Franco, C. A. (2018). Effect of the asphaltene oxidation process on the formation of emulsions of water in oil (W/O) model solutions. *Energies,* 11(4), 1–21. https://doi.org/10.3390/en11040722

Nikodinovic-Runic, J., Coulombel, L., Francuski, D., Sharma, N. D., Boyd, D. R., Ferrall, R. M. O., & O'Connor, K. E. (2013). The oxidation of alkylaryl sulfides and benzo [b] thiophenes by Escherichia coli cells expressing wild-type and engineered styrene monooxygenase from Pseudomonas putida CA-3. *Applied microbiology and biotechnology,* 97, 4849-4858. https://doi.org/10.1007/s00253-012-4332-5

Maddams, W. F. (1980). The Scope and Limitations of Curve Fitting. *Applied Spectroscopy,* 34(3), 245–267. https://doi.org/10.1366/0003702804730312

Martín-Martínez, F. J., Fini, E. H., & Buehler, M. J. (2015). Molecular asphaltene models based on Clar sextet theory. *Rsc Advances*, 5(1), 753-759. https://doi.org/10.1039/C4RA05694A

Medina, O. E., Gallego, J., Rodríguez, E., Franco, C. A., & Cortés, F. B. (2019). Effect of pressure on the oxidation kinetics of Asphaltenes. *Energy & Fuels,* 33(11), 10734-10744. https://doi.org/10.1021/acs.energyfuels.9b02611

Moncayo-Riascos, I., Rojas-Ruiz, F. A., Orrego-Ruiz, J. A., Cundar, C., Torres, R. G., & Cañas-Marín, W. (2022). Reconstruction of a synthetic crude oil using petroleomics and molecular dynamics simulations: A multistructural approach to understanding asphaltene aggregation behavior. *Energy & Fuels,* 36(2), 837-850. https://doi.org/10.1021/acs.energyfuels.1c03497

Mullins, O. C., Sabbah, H., Eyssautier, J., Pomerantz, A. E., Barré, L., Andrews, A. B., ... & Zare, R. N. (2012). Advances in asphaltene science and the Yen–Mullins model. *Energy & Fuels,* 26(7), 3986-4003. https://doi.org/10.1021/ef300185p

Nagiev, T. M. (2007a). Conjugated Reactions of Oxidation with Hydrogen Peroxide in the Gas Phase. *Coherent Synchronized Oxidation Reactions by Hydrogen Peroxide* (pp. 91–145). https://doi.org/10.1016/B978-044452851-3/50005-4

Nagiev, T. M. (2007b). Kinetics and the Mechanism of Synchronous (Interfering) Reactions of Hydrogen Peroxide Dissociation and Oxidation of Substrates in the Gas Phase. *Coherent Synchronized Oxidation Reactions by Hydrogen Peroxide* (pp. 147–184). https://doi.org/10.1016/B978-044452851-3/50006-6

Ok, S., & Mal, T. K. (2019). NMR Spectroscopy Analysis of Asphaltenes. *Energy and Fuels,* 33(11), 10391–10414. https://doi.org/10.1021/acs.energyfuels.9b02240

Oldham, D., Qu, X., Wang, H., & Fini, E. H. (2020). Investigating Change of Polydispersity and Rheology of Crude Oil and Bitumen Due to Asphaltene Oxidation. *Energy and Fuels,* 34(8), 10299–10305. https://doi.org/10.1021/acs.energyfuels.0c01344

Orrego, J. A., Cabanzo Hernández, R., & Mejía-Ospino, E. (2010). Structural study of colombian coal by fourier transform infrared spectroscopy coupled to attenuated total reflectance (FTIR-ATR). *Revista mexicana de física,* 56(3), 251-254. https://www.scielo.org.mx/pdf/rmf/v56n3/v56n3a11.pdf

Orrego-Ruiz, J. A., García, R., Cundar Paredes, C. D., & Rojas-Ruiz, F. A. (2022). Characterization of Acid Species in Asphaltenic Fractions by Fourier Transform Ion Cyclotron Resonance Mass Spectrometry and Infrared Spectroscopy. *Energy & Fuels,* 36(24), 14852-14864. https://doi.org/10.1021/acs.energyfuels.2c03219

Orrego-Ruiz, J. A.; Guzman, A.; Molina, D.; Mejía-Ospino, E.´. (2011). Mid-infrared Attenuated Total Reflectance (MIR-ATR) Predictive Models for Asphaltene Contents in Vacuum Residua: Asphaltene Structure-Functionality Correlations Based on Partial Least-Squares Regression (PLS-R). *Energy Fuels,* 25, 3678–3686. https://doi.org/10.1021/ef200834x

Orrego-Ruiz, J. A., Molina, D., Mejía-Ospino, E., & Guzmán, A. (2015). Understanding the Molecular Information Contained in the Infrared Spectra of Colombian Vacuum Residua by Principal Component Analysis. *Analytical Methods in Petroleum Upstream Applications,* 275-300. https://doi.org/https://doi.org/10.1201/b18109

Poveda, J. C., & Molina, D. R. (2012). Average molecular parameters of heavy crude oils and their fractions using NMR spectroscopy. *Journal of Petroleum Science and Engineering*, 84, 1-7. https://doi.org/10.1016/j.petrol.2012.01.005

Prado, G. H., & de Klerk, A. (2015). Alkylation of asphaltenes using a FeCl3 catalyst. *Energy & Fuels,* 29(8), 4947-4955. https://doi.org/10.1021/acs.energyfuels.5b01292

Pudenzi, M. A., Santos, J. M., Wisniewski Jr, A., & Eberlin, M. N. (2018). Comprehensive characterization of asphaltenes by Fourier transform ion cyclotron resonance mass spectrometry precipitated under different n-alkanes solvents. *Energy & Fuels,* 32(2), 1038-1046. https://doi.org/10.1021/acs.energyfuels.7b02262

Qiyong, X., Wyclif, K., Jingjun, P., Xiong, R., Deng, W., Zhang, S., ... & Yang, Y. (2020). Analysis of Xinjiang asphaltenes using high precision spectroscopy. *RSC advances,* 10(65), 39425-39433. https://doi.org/10.1039/d0ra07278h

Ramírez-Pradilla, J. S., Rubiano, J., Rojas-Ruiz, F. A., & Orrego-Ruiz, J. A. (2024). Architecture of miscellaneous asphaltenes: A molecular odyssey. *Fuel,* 371, 132081. https://doi.org/10.1016/j.fuel.2024.132081

Rojas-Ruiz, F. A., Bottia-Ramirez, H., Rodríguez-Rodríguez, L., & Orrego-Ruiz, J. A. (2017). Exploring compositional changes along in situ combustion and their implications on emulsion stabilization via Fourier transform ion cyclotron resonance mass spectrometry (FT-ICR MS). *Energy & Fuels,* 31(11), 11995-12003. https://doi.org/10.1021/acs.energyfuels.7b02421

Russo, C., Stanzione, F., Tregrossi, A., & Ciajolo, A. (2014). Infrared spectroscopy of some carbon-based materials relevant in combustion: qualitative and quantitative analysis of hydrogen. *Carbon,* 74, 127-138. https://doi.org/10.1016/j.carbon.2014.03.014

Sánchez, N. M., & de Klerk, A. (2016a). Low-temperature oxidative asphaltenes liquefaction for petrochemicals: fact or fiction? *Applied Petrochemical Research,* 6(2), 97–106. https://doi.org/10.1007/s13203-016-0147-0

Sánchez, N. M., & de Klerk, A. (2016b). Low-temperature oxidative asphaltenes liquefaction for petrochemicals: fact or fiction? *Applied Petrochemical Research,* 6(2), 97–106. https://doi.org/10.1007/s13203-016-0147-0

Shabalin, K. V., Foss, L. E., Borisova, Y. Y., Borisov, D. N., Yakubova, S. G., & Yakubov, M. R. (2020). Study of the heavy oil asphaltenes oxidation products composition using EPR and IR spectroscopy. *Petroleum Science and Technology,* 38(22), 992-997. https://doi.org/10.1080/10916466.2020.1802484

Schuler, B., Meyer, G., Peña, D., Mullins, O. C., & Gross, L. (2015). Unraveling the Molecular Structures of Asphaltenes by Atomic Force Microscopy. *Journal of the American Chemical Society*, 137(31), 9870–9876. https://doi.org/10.1021/jacs.5b04056

Lin, S. Y., Yu, H. L., & Li, M. J. (1999). Formation of six-membered cyclic anhydrides by thermally induced intramolecular ester condensation in Eudragit E film. *Polymer,* 40(12), 3589-3593. https://doi.org/10.1016/S0032-3861(98)00488-1

Siddiquee, M. N., & De Klerk, A. (2014). Hydrocarbon addition reactions during low-temperature autoxidation of oilsands bitumen. *Energy and Fuels,* 28(11), 6848–6859. https://doi.org/10.1021/ef501694s

Siddiqui, M. N. (2009). Exploring the chemical reactivity of asphaltenes. *Prepr. Pap.-Am. Chem. Soc., Div. Fuel Chem,* 54(1), 14. https://www.academia.edu/download/90453729/download_jsessionid_54DE59439E5018BF773842504BEF5258.pdf

Spiegel, M. T., Anthony, I. G. M., Brantley, M. R., Hassell, A., Farmer, P. J., & Solouki, T. (2018). Reactivities of Aromatic Protons in Crude Oil Fractions toward Br2 Tagging for Structural Characterization by Nuclear Magnetic Resonance and Electron Paramagnetic Resonance Spectroscopy and Mass Spectrometry. *Energy and Fuels,* 32(10), 10549–10555. https://doi.org/10.1021/acs.energyfuels.8b02342

Standard, A.S.T.M D6560-22. (2022). Standard Test Method for Determination of Asphaltenes (Heptane Insolubles) in Crude and Petroleum Products ASTM International. In ASTM International. *ASTM International.* https://doi.org/10.1520/D6560-22.2

Strausz, O. P., Mojelsky, T. W., Lown, E. M., Kowalewski, I., & Behar, F. (1999). Structural features of Boscan and Duri asphaltenes. *Energy and Fuels,* 13(2), 228–247. https://doi.org/10.1021/ef980245l

Thorn, K. A., & Cox, L. G. (2015). Probing the carbonyl functionality of a petroleum resin and asphaltene through oximation and schiff base formation in conjunction with N-15 NMR. *PLoS One*, 10(11), e0142452. https://doi.org/10.1371/journal.pone.0142452

Vetrivel, S., & Pandurangan, A. (2004). Side-chain oxidation of ethylbenzene with tert-butylhydroperoxide over mesoporous Mn-MCM-41 molecular sieves. *Journal of Molecular Catalysis A: Chemical,* 217(1-2), 165-174. https://doi.org/10.1016/j.molcata.2004.03.022

Yang, Y., Chaisoontornyotin, W., & Hoepfner, M. P. (2018). Structure of asphaltenes during precipitation investigated by ultra-small-angle x-ray scattering. *Langmuir,* 34(35), 10371-10380.. https://doi.org/10.1021/acs.langmuir.8b01873

Zendehboudi, S. (2019). Chapter 3 | Asphaltenes Review: Characterization and Modeling. ASTM MANUALS. Fuels and Lubricants Handbook: *Technology, Properties, Performance, and Testing, 2th eddition.* (pp. 39–77). https://doi.org/10.1520/MNL3720160027

Zhao, B., & Shaw, J. M. (2007). Composition and size distribution of coherent nanostructures in Athabasca bitumen and Maya crude oil. *Energy & Fuels,* 21(5), 2795-2804. https://doi.org/10.1021/ef070119u

Zheng, F., Shi, Q., Vallverdu, G. S., Giusti, P., & Bouyssiere, B. (2020). Fractionation and characterization of petroleum asphaltene: focus on metalopetroleomics. *Processes,* 8(11), 1504. https://doi.org/10.3390/pr8111504

Zheng, C., Zhu, M., Zareie, R., & Zhang, D. (2018). Characterisation of subfractions of asphaltenes extracted from an oil sand using NMR, DEPT and MALDI-TOF. *Journal of Petroleum Science and Engineering,* 168, 148-155. https://doi.org/10.1016/j.petrol.2018.05.002

Zojaji, I., Esfandiarian, A., & Taheri-Shakib, J. (2021). Toward molecular characterization of asphaltene from different origins under different conditions by

means of FT-IR spectroscopy. Advances in *Colloid and Interface Science*, 289, 102314. https://doi.org/10.1016/j.cis.2020.102314

Zuo, P., Qu, S., & Shen, W. (2019). Asphaltenes: Separations, structural analysis and applications. *Journal of Energy Chemistry*, 34, 186-207. https://doi.org/10.1016/j.jechem.2018.10.004

AUTHORS

Fernando A. Rojas-Ruiz
Affiliation: ECOPETROL, Instituto Colombiano del Petróleo y energías de la transición ICPET, Piedecuesta, Santander ColombiORCID: https://orcid.org/0000-0002-3566-9498
e-mail: fernandoa.rojas@ecopetrol.com.co

Diego R. Merchan-Arenas
Affiliation: ECOPETROL, Instituto Colombiano del Petróleo y energías de la transición ICPET, Piedecuesta, Santander Colombia
ORCID: https://orcid.org/0000-0001-9243-5914
e-mail: diego.merchan@ecopetrol.com.co

Santiago Villabona Estupiñan
Affiliation: DTH, Piedecuesta, Colombia
ORCID: https://orcid.org/0000-0003-2431-1906
e-mail: tiagovillabona@hotmail.com

Juan S. Ramírez-Pradilla
Affiliation: ECOPETROL, Instituto Colombiano del Petróleo y energías de la transición ICPET, Piedecuesta, Santander Colombia
ORCID: https://orcid.org/0000-0001-7937-2322
e-mail: juanse.ramirez@ecopetrol.com.co

Jorge A. Orrego Ruiz
Affiliation: ECOPETROL, Instituto Colombiano del Petróleo y energías de la transición ICPET, Piedecuesta, Santander Colombia
ORCID: https://orcid.org/0000-0002-9087-1074
e-mail: jorge.orrego@ecopetrol.com.co

How to cite: Rojas, et al., (2024). Structural insights of asphaltenes through mild oxidation reactions and MID infrared spectroscopy. *Ciencia, Tecnología y Futuro* - CT&F. Vol. 14 No. 2, 29 - 44.